Compressibility Studies of Copper Selenides Obtained by Cation Exchange Reaction Revealing the New CsCl Phase

Progna Banerjee[1]*, Vitali B. Prakapenka[4], Stella Chariton[4] & Elena V. Shevchenko[1,2,3]*

[1]Center for Nanoscale Materials, Argonne National Laboratory, Argonne, Illinois 60439, USA

[2]Department of Chemistry and [3]James Franck Institute, University of Chicago, Chicago, Illinois 60637, USA

[4]Center for Advanced Radiation Sources, The University of Chicago, Chicago, Illinois 60637, USA

* Corresponding authors

*Emails: prognaphysics@gmail.com eshevchenko@anl.gov

KEYWORDS. cation exchange reaction, copper selenide, diamond anvil cell, cubic symmetry, triangular pyramidal faceted nanocrystal, nanoplatelet

ABSTRACT

In this study, we conducted a comprehensive high-pressure investigation on zinc blende $Cu_{2-x}Se$ nanostructures synthesized via cation exchange reactions (CERs) from CdSe NCs, exhibiting two distinct morphologies: zinc blende faceted nanocrystals (NCs) and wurtzite nanoplatelets (NPLs). By employing the diamond anvil cell (DAC) technique, we analyzed the phase transitions in $Cu_{2-x}Se$ NCs with B1 phase (*Fm-3m* symmetry) under compression up to 40 GPa. Remarkably, we observed structural transformations that deviate from those observed in zinc blende CdSe NCs and in bulk $Cu_{2-x}Se$. Specifically, a novel CsCl-type lattice (B2 phase) with *Pm-3m* symmetry emerged above 4 GPa, a phase previously unobserved experimentally in copper selenides. Notably, the CsCl-type lattice of $Cu_{2-x}Se$ NCs exhibited partial retention upon decompression. We studied the influence of morphology and shape uniformity on the structural stability of nanostructures. This understanding of the phase behavior in copper selenides is imperative for realizing their full potential in forthcoming applications. Furthermore, the identification of a previously unknown phase in the extensively studied nanomaterial, copper selenide, represents a significant milestone in the ongoing exploration of novel material phases that may offer distinct and valuable properties.

INTRODUCTION

Understanding the stability of the structure constitutes a crucial aspect in ascertaining the ideal design and applications of nanocrystals (NCs).[1-4] The study of phase transitions under extreme conditions[5, 6] has been instrumental in unraveling the fundamental properties and behaviors of various chalcogenide-based nanomaterials. High pressure can induce reversible or irreversible phase transformations in nanostructures[7-9] as well as to lead to their morphological changes resulting in the synthesis of nanowires from quasi-spherical NCs[1]. Moreover, new phases of NCs (e.g. orthorhombic MnP-type MnS) that do not exist in bulk counterparts can be fabricated under high pressure[9].

CdSe and CdS nanostructures are among the most studied nanosized systems[7, 10-13] in terms of their phase and morphology stability under pressure. The wurtzite CdSe NCs were consistently reported to undergo a size-dependent irreversible structural transformation to cubic rock salt at pressures above 6 GPa[11, 14], which are higher than pressure leading to the phase transformations in bulk CdSe (~ 3 GPa). Upon decompression, the rock salt CdSe NCs transform into mixed wurtzite and zinc blende phase[12, 15]. Similarly, irreversible phase transition was reported for hexagonal wurtzite CdS NCs from pressure-induced rock salt phase[1]; however, cubic zinc blende CdSe NCs seemed to revert to the initial phase from rock salt after decompression[3].

Both zinc blende and wurtzite CdSe NCs were shown to be an excellent hosts for synthesis of NCs with different compositions via cation exchange reactions (CERs) enabling the fabrication of phases that cannot be prepared via direct synthesis[16]. Cation exchange reactions[25] under ambient conditions are recognized as a promising post-synthetic strategy to tune the chemical composition[17, 18] of NCs maintaining morphology[19-22], structure and dimensions[23-25]. CERs enable design of new complex structures including those with metastable phases[20, 26] through the

preservation of the anionic framework[27]. The extent of the CER as well as the resulting structures depend[31,32] on the chemical nature of the guest cation, their ionic radii and oxidation states and the choice of ligands and solvation environments[33]. CERs in CdSe NCs[20, 21] with zinc blende and wurtzite structures were used to synthesize zinc blende $Cu_{2-x}Se$ NCs that can reveal superionic properties meaning desirable thermoelectric properties quantified by high Seebeck coefficient[28-31] and low thermal conductivity[32] as well as other interesting optoelectronic[21] properties. Copper selenides can exist in a variety of compositions, each with their unique crystal structure[33], opto-electronic signals[34], plasmonic resonance features[21, 35, 36] and other emergent properties[37, 38].

Here we performed the comprehensive high-pressure study on zinc blende $Cu_{2-x}Se$ NCs obtained via direct ambient temperature and pressure CER transformations in CdSe NCs with two morphologies such as triangular zinc blende nanopyramids, and hexagonal wurtzite nanoplatelets (NPLs). Using the diamond anvil cell (DAC) technique[17–19] we analyzed the phase transitions in $Cu_{2-x}Se$ NCs upon compression up to 40 GPa and found structural transformations that are different from transformations reported in corresponding host CdSe NCs. Thus, we found a new CsCl-like structure (B2 phase) with *Pm-3m* symmetry formed above 4 GPa that has never been observed experimentally. The B2 phase of $Cu_{2-x}Se$ NCs is partially preserved upon decompression. We discussed the effect of shape and shape uniformity on structural stability. Understanding the phase behavior in copper selenides is essential for unlocking their full potential in their future applications[16, 39] considering that several phases of chalcogenides (e.g. silver, bismuth and antimony selenides and tellurides, etc.) exhibited three-dimensional topological insulating[40, 41] properties. Understanding of the experimental conditions favoring the formation of a particular phase for the system with a very rich phase diagram such as copper-selenide is important for further progress in predictive synthesis[16]. Moreover, the observation of a new phase of intensively studied

nanomaterial such as copper selenide is an important step in further exploration of the new phases[16] of materials that can potentially offer unique properties.

RESULTS AND DISCUSSIONS:

A. CER in faceted CdSe NCs under anaerobic conditions with Cu(I) precursor

CdSe NCs with faceted triangular pyramidal morphology (**Figure 1a and inset**) were synthetized using a modified procedure reported in literature[34]. A detailed description of the synthetic procedure is provided in the Methods. The starting amount of the CdSe NCs was 340 nmol in 3 mL total of toluene as calculated from the absorption spectrum in **Figure 1b** using Beer-lambert's law. The degree of cation exchange in these NCs upon addition of different amounts of Cu(I) precursor was monitored via optical absorption (**Figure 1b**) and photoluminescence emission experiments (**Figure 1c**). The CdSe *hh* (heavy hole) exciton peak gradually disappear with the addition of the Cu(I) precursor such as tetrakis(acetonitrile) copper hexafluorophosphate under nitrogen atmosphere reaching a featureless band edge characteristic to copper selenide upon addition of 990 nmol of Cu(I) (**Figure 1b)**. Photoluminescence spectra show that quenching of photoluminescence signal of CdSe occurs upon addition of 770 nmol of Cu(I) precursor **(Figure 1c)**, when features of CdSe are still present in UV/Vis spectrum (**Figure 1b**).
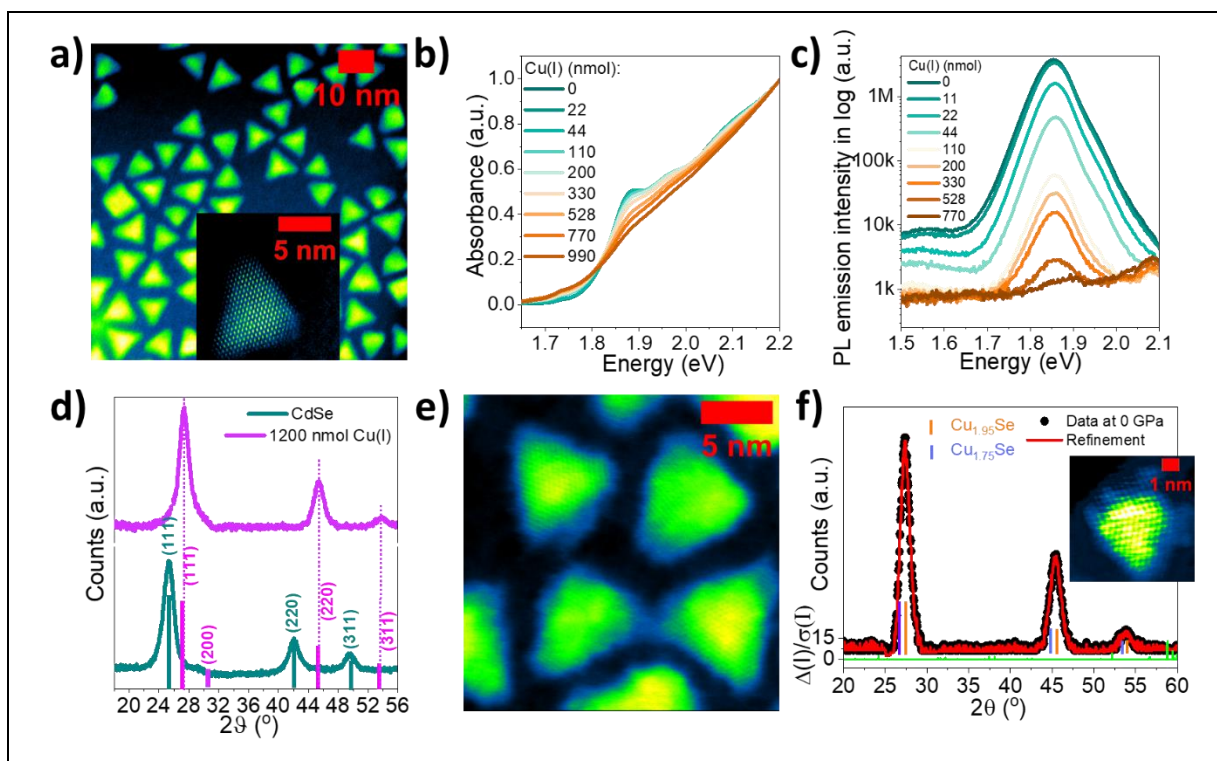
Figure 1. (a) The STEM image of CdSe faceted NCs with faceted triangular pyramidal nanocrystal morphologies. The inset in (a) is high resolution STEM image of an individual CdSe nanopyramid. The evolution of (b) UV/Vis and (c) photoluminescence emission spectra acquired upon addition of different amounts of Cu(I) precursor for 3 h. (d) XRD indicating the complete transformation from zinc blende CdSe to $Cu_{2-x}Se$ at ambient pressure with preserved morphology and structure. (e) The STEM image of $Cu_{2-x}Se$ NCs obtained via CERs in CdSe NCs shown in (a). (f) Rietveld refinement analysis (red pattern) performed on XRD data obtained at the final stage (black scatter for raw data) at room pressure proves the zinc blende $Cu_{1.95}Se$ (orange ticks) to be the primary phase, with $Cu_{1.75}Se$ being the secondary phase (purple ticks). Inset in (f) shows the representative high resolution STEM image of the pyramidal $Cu_{2-x}Se$ NCs.

The X-ray diffraction (XRD) patterns in **Figure 1d** show the transformation of CdSe (light blue pattern) with zinc blende structure to $Cu_{2-x}Se$ (pink pattern). The XRD pattern obtained from the final stage of the reaction can be matched closely with the $Cu_{1.95}Se$ reference pattern, with the Cu cation occupancies modified slightly from JCPDS card 71-0044 for $Cu_{1.8}Se$. The morphology of the NCs at the final stage in **Figure 1e** is similar to that of the CdSe NCs. The Rietveld refinement analysis on the powder XRD (pXRD) pattern of the end-product in **Figure 1f** reveals zinc blende phase with compositions of $Cu_{1.75}Se$ (9%, purple ticks) and predominantly $Cu_{1.95}Se$

(91%, orange ticks), both with *Fm-3m* symmetries. **Figure 1f inset** showing a single triangular pyramidal NC of $Cu_{1.95}Se$ composition demonstrate slip boundaries, corresponding to symmetry breaking of the (100) basal planes[42].

The site coordination information for the various compositions and crystal structures detected using the Rietveld refinement reveals that Cu atoms are placed exclusively in the tetrahedral *8c* and trigonal *32f* interstitial positions in the $Cu_{1.75}Se$ (lattice constant: 5.6756 Å) and $Cu_{1.95}Se$ (lattice constant: 6.1769 Å), respectively. The Cu cation placement in these cubic *Fm-3m* structures would suggest a low temperature non-superionic structure[7], where the eight tetrahedral sites are not completely full to avoid the high energy configuration formed through the ensuing *Cu$^+$-Cu$^+$* repulsion. Instead, a percentage of Cu cations are placed in the trigonal positions.

The more Cu-deficient tetragonal Cu_3Se_2 structure for example, matching the JCPDS card 65-1656 (lattice constants: a = 6.4024 Å and c = 4.2786 Å respectively) with *P-42$_1$m* symmetry has Cu in the *2a* and *4e* interstitial sites. Another non zinc-blende cubic *F23* phase of Cu_2Se with higher Cu content (lattice constant: a = 5.84 Å) of low-temperature α-Cu_2Se[33, 43, 44] with JCPDS card identifier 76-0136 contains Cu in the tetrahedral *4c*, octahedral *4b*, and the trigonal *16e* sites respectively. Occasionally other copper deficient phases may be present in synthesized copper selenides -such as Cu_3Se_2 and $CuSe$-which prompted us to check for the presence of these phases in our samples. The tetragonal Cu_3Se_2 phase in particular, was found to be formed upon aging of the $Cu_{2-x}Se$ sample under ambient conditions in a previous study[45], with highest electrical conductivity values recorded from the Cu-deficient vacancy-rich $Cu_{2-x}Se$ samples. We do not observe the presence of the Cu_3Se_2 or Cu_2Se phases.

It is worth noting that under ambient pressure zinc blende phase of $Cu_{2-x}Se$ is realized to the best of our knowledge in only NCs obtained via CERs, while the[46] most common crystal structures

reported in the literature for $Cu_{2-x}Se$ NCs synthetized via direct synthesis[16, 35, 47, 48] are berzelianite (cubic, space group $Fm\overline{3}m$) and metastable weissite-like $Cu_{2-x}Se$ (trigonal, space group $P\overline{3}m1$) and wurtzite-like $Cu_{2-x}Se$ (hexagonal, space group $P6_3mc$). Direct synthesis often results in the formation of mixed phases, while CER is a suitable post-synthetic method to isolate singular phases[20, 21] of copper selenides from nanostructured templates and hence utilized in our studies.

B. DAC study on $Cu_{2-x}Se$ NCs

The high-pressure synchrotron X-ray diffraction experiments were performed on $Cu_{2-x}Se$ NCs dried from the colloidal organic solvent, mounted into the diamond anvil cell setup with Ne as the pressure transmitting medium. The diffraction patterns from 2 GPa up to 40 GPa applied pressure on the $Cu_{2-x}Se$ NCs shown in **Figures 2a and b** indicate that zinc blende phase with predominantly $Cu_{1.95}Se$ compositions undergo a phase transformation to CsCl-type lattice (B2 phase) with *Pm-3m* symmetry. This phase transition behavior is observed for the first time in copper selenides. As is shown in **Figure 2a** the structural changes occur at around 5 GPa. Between 5 to 7 GPa applied pressure, both the zinc blende and CsCl-type lattice co-exist simultaneously. After 9 GPa, the CsCl-type lattice is preserved in the NCs up to 40 GPa (**Figure 2b**). Pressure-induced phase transition to CsCl-type phase has been observed typically in oxides[49] and has been partially attributed to repulsion between anions resisting the structural compressive changes in the anion-rich layers[50].

The XRD pattern acquired at 2 GPa is refined into cubic $Cu_{1.95}Se$ composition, with lattice constant a = 5.9849 Å, which is compressed by 15.6% from the cell dimensions calculated at ambient pressure in **Figure 1d**. The new peaks start to appear at ~5 GPa in addition to peaks characteristic to cubic $Cu_{1.95}Se$ (**Figure 2a**). The new phase is identified as B2 phase with *Pm-3m*

symmetry (**Figure 2a, b**) The absence of a noticeable broadening of the peaks corresponding to the cubic $Cu_{1.95}Se$ indicates that the new phase does not nucleate within the volume of NCs with zinc blende structure. It is worth noting that phase transformation in NCs appears to proceed through a single nucleation event[4, 6]. In fact, this observation rather points to the presence of some NCs that undergo pressure-mediated nucleation followed by subsequent structural reconstruction to B2 phase at an earlier stage. In the pressure range between 2 and 7 GPa, very little change in peak broadening is observed for the (111) peak (**Figure S1**). Unlike bulk, further pressure increase up to 40 GPa is not associated with any other structural transitions in NCs, and XRD peaks characteristic of B2 phase monotonically shift as a result of lattice compression(**Figure 2b**). The acquired 2D patterns are presented in **Figure 2c** for applied pressure of 2, 3.5, 5, 6.5, 7 and 9 GPa, respectively. Once the pressure is released, the structure is partially returned to cubic zinc blende $Cu_{1.95}Se$ while some B2 phase is preserved (**Figure 2d)**.
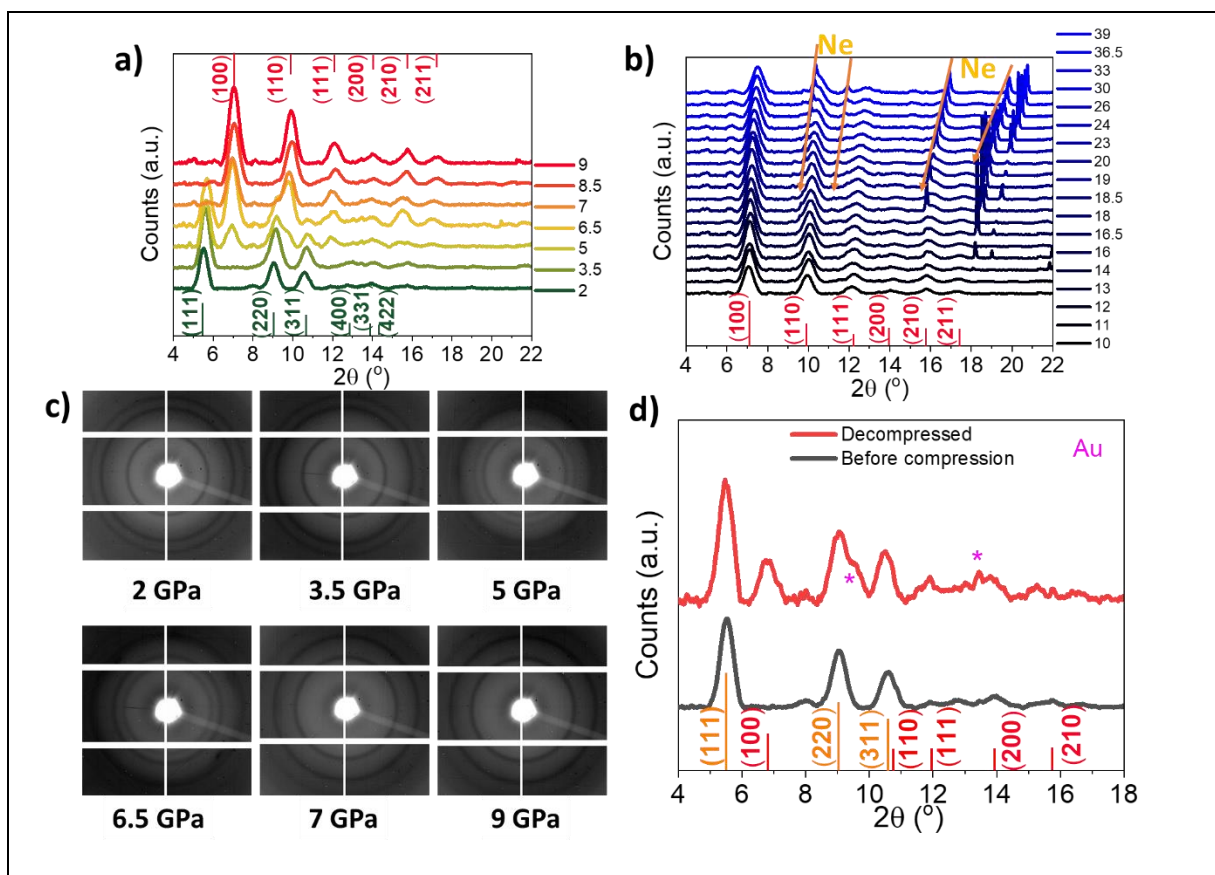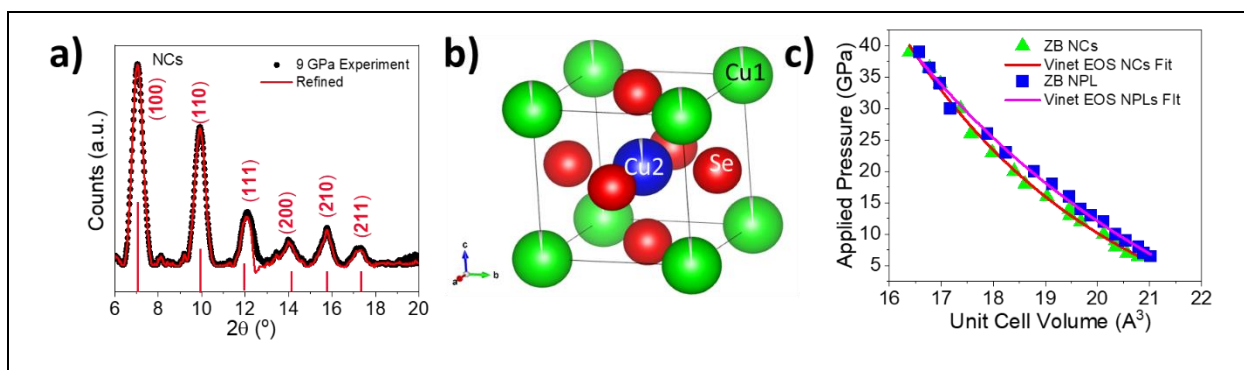
Figure 2. (a) The diffraction patterns of $Cu_{2-x}Se$ NCs measured at 2, 3.5, 5, 6.5, 7, 8.5 and 9 GPa(the legend on the right indicates the applied pressure). (b) The diffraction patterns for the $Cu_{2-x}Se$ NCs transformed to CsCl-type phase measured in10-40 GPa (the legend on the right indicates the applied pressure). The sharp peaks at ~10 & 11.4 º 2θ respectively, starting at 19 GPa and red shifting until the end of the compression experiment belong to Ne that is used for pressure calibration and appear as a result of the sample's movement during compression. (c) The acquired 2D patterns obtained at applied pressure of 2, 3.5, 5, 6.5, 7 and 9 GPa, respectively. (d) The XRD patterns measured at 2 GPa at the start of compression (grey pattern) and after pressure release on the same sample (red pattern). Reference zinc blende B1 (*Fm-3m*) and CsCl-type (*Pm-3m*) peaks are represented as orange and red markers on the x-axis respectively. The pink peaks denoted by * correspond to Au that was used to monitor the pressure in DAC experiments (note, that the sample can move during compression and decompression).

We performed Rietveld refinement fitting of diffraction pattern obtained at 9 GPa where complete phase transformation took place (**Figure 3a**). The predominant phase is $Cu_{1.95}Se$ with $Cu_{1.75}Se$ being the secondary phase. The crystal structure simulated through the fittings is

represented in **Figure 3b**. The CIF file for the CsCl-type structure obtained through simulations on the NCs is provided as a supplementary file. The CsCl-type structure is partially preserved in the studied samples upon decompression. In fact, the pattern obtained upon decompression resembles the pattern of $Cu_{2-x}Se$ sample at 5 GPa. The pattern upon decompression is shifted from the 5 GPa pattern and the peak positions corresponding to zinc blende phase of $Cu_{2-x}Se$ coincide with peak positions of $Cu_{2-x}Se$ sample obtained under ambient pressures before the compressionf. This observation points out that the CsCl-type can be stabilized for a fraction of samples, and it can depend on the morphology and/or size of the NCs. The analysis of the width of XRD peaks shown in **Figure S1** shows the (111) peak monotonically broadening with applied pressure between 2 and 7 GPa, hence there is not much change in NC size in this range.

High pressure studies on bulk materials at room-temperature were previously performed on common for bulk phase of Cu_2Se such as monoclinic (*C2/c*), demonstrating its transformation into another monoclinic phase with *C2/m* symmetry at ~3.3 GPa and bulk metallic with *Pca2₁* symmetry at 7.4 GPa [51].

Figure 3. (a) Rietveld refinement performed on the $Cu_{2-x}Se$ NC for diffraction pattern obtained at an applied pressure of 9 GPa. The simulated CsCl-type (*Pm-3m*) structure is visualized in (b). The blue and green correspond to Cu in the 1*a* and 1*b* positions, and red dots correspond to Se atoms in 3*c* position, respectively. The volume vs pressure curves are shown in (c) for both NCs (green symbols) and NPLs (blue symbols), with the Vinet EoS fit shown in red/pink for NCs/NPLs, respectively.

We also explored the structural stability of $Cu_{2-x}Se$ NCs prepared via CERs in CdSe NPLs with hexagonal wurtzite crystal structure. Wurtzite CdSe NPLs consisting of 4 monolayers (4 ML) were synthetized following the previously published procedure[52] (**Figure S2a**). CERs in wurtzite CdSe NPLs transformed them into $Cu_{2-x}Se$ of similar morphology (**Figure S2b**). The XRD pattern of the end-product is $Cu_{2-x}Se$ with cubic zinc blende symmetry is displayed in **Figure S3a**. The end product of CER contains little to no Cd, and Cu and Se in the ratio of $Cu_{1.95}Se$, as calculated from the energy dispersive spectroscopy (EDS) measurements (**Figure S2** panels **c-f**). Interestingly, the crystal symmetry was transformed from hexagonal wurtzite to cubic zinc blende as a result of CERs to reach the lowest energy configuration for the $Cu_{2-x}Se$ composition[16, 33]. Similarly, to $Cu_{2-x}Se$ NCs, Rietveld refinements on the $Cu_{2-x}Se$ NPLs reveal cubic phases with predominantly $Cu_{1.95}Se$ with small amount (~5%) of $Cu_{1.75}Se$ with the same crystal symmetry. The lattice constant for the $Cu_{1.95}Se$ is a = 5.8366 Å and the Cu is present in the tetrahedral $8c$ and trigonal $32f$ interstitial positions; with the direct Cu-Cu bonding absent. The lattice constant for the $Cu_{1.75}Se$ is a = 5.7283 Å and the Cu is present in the tetrahedral $8c$ and trigonal $32f$ interstitial positions.

High pressure studies demonstrated that zinc blende $Cu_{2-x}Se$ NPLs obtained using wurtzite CdSe host underwent a similar phase transformation (**Figure S3b**) from zinc blende to the CsCl-type B2 phase. No further changes in phase are observed from 7 to 40 GPa. Fitting of the compression data in the pressure range supporting the CsCl-type B2 phase for both $Cu_{2-x}Se$ NCs and NPLs shown in Figure **3c** using the Vinet equation of state[6, 53-55] (EoS) provides the bulk modulus value for $Cu_{2-x}Se$ NCs and NPLs as B_{NCs} = 59.7 +/- 13.2 GPa with B' = 4.56 +/- 0.9 GPa and B_{NPLs} = 84.3 +/- 14.7 GPa with B' = 2.41 +/- 0.8 GPa, respectively. The higher bulk modulus obtained for CsCl-type $Cu_{2-x}Se$ NPLs can be associated with their shape. Previously, it was shown

that CdSe NPLs exhibited a higher phase transition as compared to other shapes of CdSe NCs[56]. Also enhanced structural stability and elastic strength were reported for CdSe nanosheets[15].

The Vinet equation of state is shown below:

$$P = 3B_0 \left(\frac{V}{V_0}\right)^{-\frac{2}{3}} \left[1 - \left(\frac{V}{V_0}\right)^{\frac{1}{3}}\right] \exp\left[X\left\{1 - \left(\frac{V}{V_0}\right)^{\frac{1}{3}}\right\}\right]$$
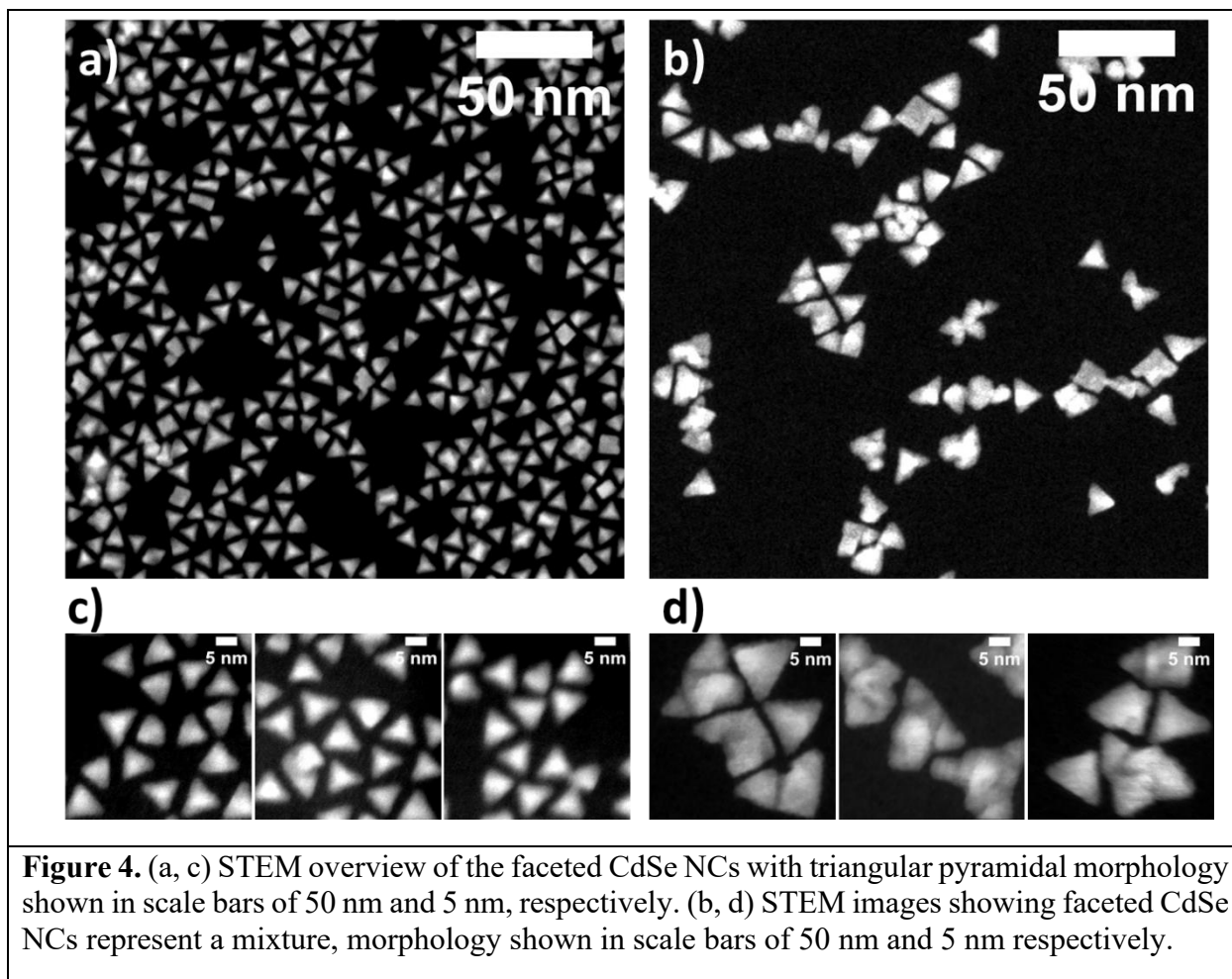
Where, B_0 and $B_0{'}$ are the bulk modulus and its first order pressure derivative at = initial pressure P (the onset of the phase transition ~6.5 GPa in our studies), respectively), and $X = \frac{3}{2}(B_0' - 1)$.

Therefore, we conclude that for $Cu_{2-x}Se$ NCs prepared via CERs regardless of their crystalline structure of the initial host CdSe NCs, pressure induced transition from zinc blende to CsCl-type B2 phase is rather general.

To understand the origin of coexistence of both cubic phases such as zinc blende and CsCl in the pressure range between 5 and 7 GPa in $Cu_{2-x}Se$ NCs shown in **Figure 2a**, we performed a detailed transmission electron microscopy (TEM) investigation of faceted CdSe NCs that were used as a host for synthesis of $Cu_{2-x}Se$ NCs. Previous studies indicated that CERs conducted under inert atmosphere in CdSe templates do not noticeably affect the morphology of the host NCs[19, 21]. Since rather extensive washing required for preparation of $Cu_{2-x}Se$ NCs suitable for the TEM analysis results in clustering of NCs on the TEM grid upon drying, therefore, we focused the morphology analysis on the CdSe NCs used as host NCs (**Figure 4**). Analysis of the TEM data pointed out the presence of NCs that can be divided into two classes: smaller sized faceted triangular nanopyramids presented of CdSe NCs (**Figure 4 a, c**) and larger nanostructures with

more complex shapes(**Figure 4 b, d**). The formation of more complex morphologies can originate from single stacking faults and facet-ligand pairing effects[42].

Previous studies on a variety of NCs demonstrated the size dependance of the phase transition upon compression[4]. The general trend of higher pressure required to overcome the nucleation barrier and cause a phase transition in the case of smaller NCs was reported[11]. This is attributed to the lower concentration of the defects in NCs as compared to larger structures as well as to higher surface energy in nanostructures. Since we have a population of smaller and larger $Cu_{2-x}Se$ NCs, it is reasonable to suggest that they experience phase transformation at different pressures. Smaller $Cu_{2-x}Se$ NCs can undergo phase transformations at a higher applied pressure as it was shown in previous studies for a variety of different types of NCs[11, 57]. We also would like to mention that EDS analysis (**Figure S4 a-c**) reveals the traces of Cd at the surface of $Cu_{2-x}Se$ NCs (**Figure S4 panel b**) meaning that extracted cadmium cations either bound to the surface or attach to the surface because of drying that, in principle, might have some effect on the onset pressure causing the phase transformation due to effect of the surface ligands on the surface energy. Previous studies indicated that elastic strength can be correlated with the presence of surface-bonded soft organic ligands[15]. Also, lattice distortion of NCs was shown to be driven by organic ligand-induced tensile strain in the case of PbS[56]. However, such effects in previous studies were not associated with formation of new pressured-induced phases.

Figure 4. (a, c) STEM overview of the faceted CdSe NCs with triangular pyramidal morphology shown in scale bars of 50 nm and 5 nm, respectively. (b, d) STEM images showing faceted CdSe NCs represent a mixture, morphology shown in scale bars of 50 nm and 5 nm respectively.

CONCLUSIONS

We performed a comprehensive high-pressure study on faceted zinc blende $Cu_{2-x}Se$ NCs obtained via CERs in host CdSe NCs with zinc blende and wurtzite structures. DAC experiments up to 40 GPa revealed that structural transformations in zinc blende lattice of $Cu_{2-x}Se$ are different from transformations observed in either of the zinc blende or wurtzite CdSe NCs used as host templates to synthetize $Cu_{2-x}Se$ NCs, as well as different from that of the bulk $Cu_{2-x}Se$. While the initial phase and the new pressure-induced phases are different for the previously reported bulk Cu_2Se, in our studies we observe the similar trend of higher onset of pressure for the first transformation at 3.3 GPa (as previously reported-3.3 GPa for nano[12] vs 4.5 GPa for bulk[11, 16]).

14

The application of pressure above 4 GPa induces the structural transformation of zinc blende $Cu_{2-x}Se$ NCs to a new CsCl-type lattice. The heterogeneity of phase transition between 2-7 GPa in NCs can be explained by the shape inhomogeneity of the studied samples. The CsCl-type (B2 phase) of $Cu_{2-x}Se$ NCs is partially preserved upon decompression. The bulk modulus for the new B2 phase of $Cu_{2-x}Se$ formed upon compression is determined to be ~59 and 84 GPa for the faceted NCs and NPLs, respectively. The exploration of phase transitions in $Cu_{2-x}Se$ prepared via CERs under high pressure using the DAC technique offers a promising avenue for advancing our understanding of their properties and behaviors. The control of pressure-induced phase transitions allows for the manipulation of structural, electronic, and optical properties, offering exciting possibilities for developing advanced functional materials. Even though different phases in copper selenides were synthesized previously using direct hot injection techniques, and cation exchange reactions, CsCl phase has not been previously obtained. Interestingly, we obtain the same CsCl like phase on both faceted $Cu_{2-x}Se$ NCs NCs and NPLs that were prepared using corresponding CdSe host nanostructures with zinc blende and wurtzite crystal lattices. Understanding of the full potential of the structural transformations is important for the better understanding over the reaction parameters and, hence, the structural space that can be accessed using high-throughput computational and synthetic methods.

METHODS

Chemical reagents. Cadmium nitrate tetrahydrate (99.997%), sodium myristate (≥99%), cadmium acetate dihydrate ($Cd(OAc)_2.2H_2O$), selenium powder (Se, ≥99.5%), octadecene (ODE; 90%), oleyl amine (OLAm, 90%), octylamine (OCAm, 95%), oleic acid (OlAc, 90%), tetrakis (acetonitrile) copper(I) hexafluorophosphate, toluene (98%), trioctylphosphine (TOP, 99%), anhydrous acetonitrile (99.8%), anhydrous ethanol, hexane (95%) and methanol were purchased from Sigma Aldrich. All chemicals were used without further purification.

Synthesis of ZB Cadmium Selenide NCs emitting at 667 nm. 78.4 mg (1 mmol) of Se powder and 15 mL of ODE were loaded into a 50 mL three-neck flask, put under vacuum at 150 °C for 2

h, refilled with N_2 atmosphere, and then heated to 280 °C for 45 min to get a light-yellow solution. Next, 266 mg of $Cd(Ac)_2 \cdot 2H_2O$ with 5 mL of oleic acid were mixed together in a 25 mL three-neck flask and heated to 150 °C under vacuum to get a transparent solution. This flask was switched to N_2 and the mixture was swiftly added to the Se stock solution with a 14-gauge needle at once. The temperature initially dropped to approximately 248 °C after the Cd-precursor solution was added, and then it quickly raised to about 260 °C by adjusting the power of the heating mantle while using insulating wool around the flask. The temperature was maintained at 265 °C for the growth of the NCs for the next 40 mins. Next, heating was discontinued, the solution was cooled rapidly with a heat gun in the cool air mode, and 1:1 v/v ethanol was added to the reactive solution to precipitate the NCs. This mixture was centrifuged at 6000 rpm for 10 mins to collect the precipitate and discard the supernatant. The CdSe NCs were redissolved in 40 mL n-hexane, to which 10 mL of ethanol was added and the centrifugation was repeated at 6000 rpm to collect the precipitate.

Synthesis of WZ Cadmium Selenide NPLs. This synthesis was reproduced from literature[52] with slight modifications. 1.23 g of $Cd(NO_3)_2 \cdot 4H_2O$ was dissolved in 40 mL of methanol, and 3.13 g of Na(myristate) was dissolved in 250 mL of methanol. Then, the two solutions were mixed, and the resulting precipitate of $Cd(myristate)_2$ was filtered. After that, the product was rinsed several times with methanol and dried under vacuum overnight. 5 mL of OLAm and 5 mL of OCAm containing 1.5 mmol (1.7 g) of $Cd(myr)_2$ were degassed for 30 min at room temperature. 4.5 mmol (0.356 g) of Se in a mixture of 2.5 mL OLAm and 2.5 mL of OCAm was injected into the solution at room temperature and then heated to 95°C for 12 hr with a heating rate of 2°C/min. Then, the sample was precipitated by adding excess ethanol containing TOP and washed repeatedly with ethanol containing TOP. At last, the precipitated powder was dispersed in toluene.

Cation exchange of NCs and NPLs under ambient conditions with Cu(I). All exchange reactions were carried out in an oxygen-free, moisture-free, N_2-filled glove box. A solution of Cu(I) precursor in the form of tetrakis(acetonitrile) copper(I) hexafluorophosphate ($[(CH3CN)4Cu]PF6$) in 10% v/v of methanol in acetonitrile was then added dropwise to either of 3 mL total volume of the 340 nmol CdSe NC/NPL solution obtained from the previous steps added in aliquots of 5 nmol under continuous stirring until the final concentration of 1200 nmol addition was reached within 3 h of start.

Optical spectroscopy measurements. Ultraviolet-visible absorption spectroscopy measurements were performed using a PerkinElmer Perkin-Elmer Lambda 950. Photoluminescence (PL) emission spectra from solutions were recorded by using Fluorolog iHR 320 Horiba Jobin Yvon spectrofluorometer equipped with a PMT detector. Cation exchange progression was monitored by ultraviolet-visible absorption spectroscopy in the visible range together with photoluminescence emission spectroscopy (excitation set at 500 nm).

X-ray diffraction measurements under ambient conditions. PXRD patterns were collected on a Bruker D2 Phaser powder X-ray diffractometer operated at full power with Cu Ka radiation wavelength (1.54 Å). Data were collected in reflection mode in the 2θ range of 15–65 º using a step size of 0.04 º with scans running for 2 h. Samples were prepared by drop-casting NCs or NPLs from solution into a thick film on a zero-background offcut Si substrate.

TEM, STEM and EDS measurements. Elemental analysis was carried out on the CdSe, the intermediate of Cu(I) reaction products at 528, 990 and 1200 nmol additions using scanning transmission electron microscopy/energy dispersive spectroscopy (STEM/EDS). STEM/EDS was performed on a Talos F200X(S)TEM instrument operating at 200 kV. Samples were prepared by drop-casting NPLs from solution onto ultrathin carbon 300-mesh Au or on 400-mesh Ni grids from Ted Pella followed by repeated washing of the grid with methanol, acetone and lastly IPA followed by drying under vacuum overnight. A zero-background double-tilt holder was used for STEM/EDS measurements. Data were collected for 40-90 min and the holder was left in the vacuum chamber overnight prior to the experiments to minimize the drift. The atomic %s of Cu, Cd and Se, obtained were converted to atomic ratios by normalizing the Se content to 1. HRTEM and HAADF-STEM images were also acquired this instrument with similar sample preparation. Size analysis was performed by measuring particle size along the long axis on HAADF-STEM images using the software, ImageJ.

DAC cell sample preparation for $Cu_{2-x}Se$ NCs and NPLs. Rhenium foil used for preparation of DAC chamber was purchased from H. Cross Company The foil was subsequently diced into 4 mm x 4 mm squares for further use as gasket chambers. The diamonds used in this study were obtained from Almax Industries. In each high-pressure experiment, an individual chunk of either the NCs or NPLs (~tens of μm in size) were extracted upon drying the colloidal solutions and loaded into a~150 μm diameter hole in a pre-indented Re gasket (chamber thickness of ~40 μm). Together with the NCs and NPLs, a small ruby fluorescent ball was loaded alongside for in-situ pressure determination. Neon (Ne) was loaded to the DAC using a pressurized gas loading system as a pressure-transmitting medium. Each NC or NPL chunk was compressed using beveled diamond anvils with either 250 and 300 μm diameter culets in two separate experiments.

High-pressure X-ray diffraction experiments at the APS synchrotron. X-ray diffraction that reveals the structure of NCs and NPLs were performed at beamline 13-ID-D of the GSECARS sector, Advanced Photon Source, Argonne National Laboratory. The X-ray beam (37 keV energy, corresponding to X-ray wavelength of $\lambda = 0.3344$ Å) was focused to a 2x3 μm^2 spot with a Kirkpatrick-Baez mirror system. In XRD experiments, DACs with both 250 and 300 μm diameter culets were used. In addition to ruby, a small flake of gold was also loaded as an additional internal pressure standard. The distance and tilting of the Pilatus3 1M Cd Te detector were calibrated using a LaB_6 NIST standard. In XRD experiments samples were compressed up to 40 GPa, with the maximum pressure set by the culet size and degree of alignment of the diamonds.

Refinement analyses of diffraction data. Refinement analyses were performed with the GSAS II software[58], and crystal structures with their simulation patterns for all phase transformations were generated with CrystalDiffract®: a powder diffraction program for Mac and Windows. CrystalMaker Software Ltd, Oxford, England (www.crystalmaker.com)

ASSOCIATED CONTENT

Supporting Information (file type PDF) contains Figures S1-S4: Peak broadening from transformation from zinc blende to B2 phase in NCs, STEM and XRD information on Cu-exchanged NPLs, and finally high-pressure diffraction patterns obtained on the $Cu_{2-x}Se$ NPLs, and STEM/EDS maps at different reaction stages with Cu(I) precursor.

Supporting file also contains the CIF information file for B2 phase of $Cu_{1.95}Se$ NCs.

AUTHOR INFORMATION

Corresponding Author

* Correspondence to: Progna Banerjee ORCID ID: 0000-0003-3257-7317

Author Contributions

P.B. conceptualized the project, performed syntheses and all characterizations, data analyses and wrote the manuscript. V.B.P. and S.C. set up the DAC high-pressure studies at the GSECARS Synchrotron at APS beamline 13-ID-D. V.B.P. helped with analyses of high-pressure diffraction patterns. E.V.S. provided project guidance and helped with analyses. All authors have given approval to the final version of the manuscript.

REFERENCES

(1) Meng, L.; Lane, J. M. D.; Baca, L.; Tafoya, J.; Ao, T.; Stoltzfus, B.; Knudson, M.; Morgan, D.; Austin, K.; Park, C.; et al. Shape Dependence of Pressure-Induced Phase Transition in CdS Semiconductor Nanocrystals. *J. Am. Chem. Soc.* **2020**, *142* (14), 6505-6510. DOI: 10.1021/jacs.0c01906.

(2) Xiao, T.; Nagaoka, Y.; Wang, X.; Jiang, T.; LaMontagne, D.; Zhang, Q.; Cao, C.; Diao, X.; Qiu, J.; Lu, Y.; et al. Nanocrystals with metastable high-pressure phases under ambient conditions. *Science* **2022**, *377* (6608), 870-874. DOI: 10.1126/science.abq7684.

(3) Lv, Y.; Yin, C.; Zhang, C.; Yu, W. W.; Wang, X.; Zhang, Y.; Xiao, M. Quantum Interference in a Single Perovskite Nanocrystal. *Nano Letters* **2019**, *19* (7), 4442-4447. DOI: 10.1021/acs.nanolett.9b01237.

(4) Meng, L.; Vu, T. V.; Criscenti, L. J.; Ho, T. A.; Qin, Y.; Fan, H. Theoretical and Experimental Advances in High-Pressure Behaviors of Nanoparticles. *Chem. Rev.* **2023**, *123* (16), 10206-10257. DOI: 10.1021/acs.chemrev.3c00169.

(5) San-Miguel, A. Nanomaterials under high-pressure. *Chem. Soc. Rev.* **2006**, *35* (10), 876-889. DOI: 10.1039/B517779K.

(6) Podsiadlo, P.; Lee, B.; Prakapenka, V. B.; Krylova, G. V.; Schaller, R. D.; Demortière, A.; Shevchenko, E. V. High-Pressure Structural Stability and Elasticity of Supercrystals Self-Assembled from Nanocrystals. *Nano Letters* **2011**, *11* (2), 579-588. DOI: 10.1021/nl103587u.

(7) Li, B.; Bian, K.; Zhou, X.; Lu, P.; Liu, S.; Brener, I.; Sinclair, M.; Luk, T.; Schunk, H.; Alarid, L.; et al. Pressure compression of CdSe nanoparticles into luminescent nanowires. *Science Advances* **2017**, *3* (5), e1602916. DOI: 10.1126/sciadv.1602916.

(8) Bai, F.; Bian, K.; Huang, X.; Wang, Z.; Fan, H. Pressure Induced Nanoparticle Phase Behavior, Property, and Applications. *Chem. Rev.* **2019**, *119* (12), 7673-7717. DOI: 10.1021/acs.chemrev.9b00023.

(9) Xiao, G.; Yang, X.; Zhang, X.; Wang, K.; Huang, X.; Ding, Z.; Ma, Y.; Zou, G.; Zou, B. A Protocol to Fabricate Nanostructured New Phase: B31-Type MnS Synthesized under High Pressure. *J. Am. Chem. Soc.* **2015**, *137* (32), 10297-10303. DOI: 10.1021/jacs.5b05629.

(10) Tolbert, S. H.; Alivisatos, A. P. Size dependence of the solid-solid phase transition in CdSe nanocrystals. *Z Phys D - Atoms, Molecules and Clusters* **1993**, *26* (1), 56-58. DOI: 10.1007/BF01429106.

(11) Tolbert, S. H.; Alivisatos, A. P. Size Dependence of a First Order Solid-Solid Phase Transition: The Wurtzite to Rock Salt Transformation in CdSe Nanocrystals. *Science* **1994**, *265* (5170), 373-376. DOI: 10.1126/science.265.5170.373.

(12) Tolbert, S. H.; Alivisatos, A. P. The wurtzite to rock salt structural transformation in CdSe nanocrystals under high pressure. *The Journal of Chemical Physics* **1995**, *102* (11), 4642-4656. DOI: 10.1063/1.469512.

(13) Pinna, N.; Weiss, K.; Sack-Kongehl, H.; Vogel, W.; Urban, J.; Pileni, M. P. Triangular CdS Nanocrystals: Synthesis, Characterization, and Stability. *Langmuir* **2001**, *17* (26), 7982-7987. DOI: 10.1021/la010287t.

(14) Jacobs, K.; Zaziski, D.; Scher, E. C.; Herhold, A. B.; Paul Alivisatos, A. Activation Volumes for Solid-Solid Transformations in Nanocrystals. *Science* **2001**, *293* (5536), 1803-1806. DOI: 10.1126/science.1063581.

(15) Wang, Z.; Wen, X.-D.; Hoffmann, R.; Son, J. S.; Li, R.; Fang, C.-C.; Smilgies, D.-M.; Hyeon, T. Reconstructing a solid-solid phase transformation pathway in CdSe nanosheets with associated soft ligands. *Proceedings of the National Academy of Sciences* **2010**, *107* (40), 17119-17124. DOI: 10.1073/pnas.1011224107.

(16) Williamson, E. M.; Sun, Z.; Tappan, B. A.; Brutchey, R. L. Predictive Synthesis of Copper Selenides Using a Multidimensional Phase Map Constructed with a Data-Driven Classifier. *J. Am. Chem. Soc.* **2023**, *145* (32), 17954-17964. DOI: 10.1021/jacs.3c05490.

(17) Petralanda, U.; De Trizio, L.; Gariano, G.; Cingolani, R.; Manna, L.; Artyukhin, S. Triggering Cation Exchange Reactions by Doping. *The Journal of Physical Chemistry Letters* **2018**, *9* (17), 4895-4900. DOI: 10.1021/acs.jpclett.8b02083.

(18) Rivest, J. B.; Jain, P. K. Cation exchange on the nanoscale: an emerging technique for new material synthesis, device fabrication, and chemical sensing. *Chem. Soc. Rev.* **2012**, *42* (1), 89-96. DOI: 10.1039/C2CS35241A (acccessed 2023/01/03/00:47:02). From pubs.rsc.org.

(19) White, S. L.; Smith, J. G.; Behl, M.; Jain, P. K. Co-operativity in a nanocrystalline solid-state transition. *Nat Commun* **2013**, *4* (1), 2933. DOI: 10.1038/ncomms3933.

(20) White, S. L.; Banerjee, P.; Chakraborty, I.; Jain, P. K. Ion Exchange Transformation of Magic-Sized Clusters. *Chem. Mater.* **2016**, *28* (22), 8391-8398. DOI: 10.1021/acs.chemmater.6b03882.

(21) White, S. L.; Banerjee, P.; Jain, P. K. Liquid-like cationic sub-lattice in copper selenide clusters. *Nat Commun* **2017**, *8* (1), 14514. DOI: 10.1038/ncomms14514.

(22) Son, D. H.; Hughes, S. M.; Yin, Y.; Paul Alivisatos, A. Cation Exchange Reactions in Ionic Nanocrystals. *Science* **2004**, *306* (5698), 1009-1012. DOI: 10.1126/science.1103755.

(23) Cho, K.-H.; Jain, P. K. Superionic Conduction in One-Dimensional Nanostructures. *ACS Nano* **2022**, *16* (8), 12445-12451. DOI: 10.1021/acsnano.2c03732.

(24) Sadtler, B.; Demchenko, D. O.; Zheng, H.; Hughes, S. M.; Merkle, M. G.; Dahmen, U.; Wang, L.-W.; Alivisatos, A. P. Selective Facet Reactivity during Cation Exchange in Cadmium Sulfide Nanorods. *J. Am. Chem. Soc.* **2009**, *131* (14), 5285-5293. DOI: 10.1021/ja809854q.

(25) Miszta, K.; Dorfs, D.; Genovese, A.; Kim, M. R.; Manna, L. Cation Exchange Reactions in Colloidal Branched Nanocrystals. *ACS Nano* **2011**, *5* (9), 7176-7183. DOI: 10.1021/nn201988w.

(26) Beberwyck, B. J.; Surendranath, Y.; Alivisatos, A. P. Cation Exchange: A Versatile Tool for Nanomaterials Synthesis. *J. Phys. Chem. C* **2013**, *117* (39), 19759-19770. DOI: 10.1021/jp405989z.

(27) Li, X.; Ji, M.; Li, H.; Wang, H.; Xu, M.; Rong, H.; Wei, J.; Liu, J.; Liu, J.; Chen, W.; et al. Cation/Anion Exchange Reactions toward the Syntheses of Upgraded Nanostructures: Principles and Applications. *Matter* **2020**, *2* (3), 554-586. DOI: 10.1016/j.matt.2019.12.024.

(28) Ashfaq, A.; Tahir, S.; Rehman, U. u.; Ali, A.; Ashfaq, H. F.; Ahmad, W.; Mushtaq, S.; Saeed, R.; Haneef, M.; Khan, K. M.; et al. Structural, morphological and thermoelectric properties of copper deficient and excessive $Cu_{2-x}S$ nanoparticles with (x=0-0.3). *Surfaces and Interfaces* **2022**, *30*, 101965. DOI: 10.1016/j.surfin.2022.101965.

(29) Li, L.; Zhao, Y.; Shi, C.; Zeng, W.; Liao, B.; Zhang, M.; Tao, X. Facile synthesis of copper selenides with different stoichiometric compositions and their thermoelectric performance at a low temperature range. *RSC Adv.* **2021**, *11* (42), 25955-25960. DOI: 10.1039/D1RA04626H.

(30) Trawiński, B.; Łapiński, M.; Kusz, B. The unstable thermoelectric effect in non-stoichiometric Cu_2Se during the non-equilibrium phase transition. *J Mater Sci* **2021**, *56* (24), 13705-13714. DOI: 10.1007/s10853-021-06170-z.

(31) Byeon, D.; Sobota, R.; Delime-Codrin, K.; Choi, S.; Hirata, K.; Adachi, M.; Kiyama, M.; Matsuura, T.; Yamamoto, Y.; Matsunami, M.; et al. Discovery of colossal Seebeck effect in metallic Cu_2Se. *Nat Commun* **2019**, *10* (1), 72. DOI: 10.1038/s41467-018-07877-5.

(32) Geng, Z.; Shi, D.; Shi, L.; Li, Y.; Snyder, G. J.; Lam, K.-h. Conventional sintered $Cu_{2-x}Se$ thermoelectric material. *Journal of Materiomics* **2019**, *5* (4), 626-633. DOI: 10.1016/j.jmat.2019.06.005.

(33) Heyding, R. D.; Murray, R. M. The crystal structures of Cu1•8Se, Cu3Se2, α- and γCuSe, CuSe2, and CuSe2II. *Can. J. Chem.* **1976**, *54* (6), 841-848. DOI: 10.1139/v76-122.

(34) Dorfs, D.; Härtling, T.; Miszta, K.; Bigall, N. C.; Kim, M. R.; Genovese, A.; Falqui, A.; Povia, M.; Manna, L. Reversible Tunability of the Near-Infrared Valence Band Plasmon Resonance in Cu2–xSe Nanocrystals. *J. Am. Chem. Soc.* **2011**, *133* (29), 11175-11180. DOI: 10.1021/ja2016284.

(35) Lord, R. W.; Fanghanel, J.; Holder, C. F.; Dabo, I.; Schaak, R. E. Colloidal Nanoparticles of a Metastable Copper Selenide Phase with Near-Infrared Plasmon Resonance. *Chem. Mater.* **2020**, *32* (23), 10227-10234. DOI: 10.1021/acs.chemmater.0c04058.

(36) Kriegel, I.; Jiang, C.; Rodríguez-Fernández, J.; Schaller, R. D.; Talapin, D. V.; da Como, E.; Feldmann, J. Tuning the Excitonic and Plasmonic Properties of Copper Chalcogenide Nanocrystals. *J. Am. Chem. Soc.* **2012**, *134* (3), 1583-1590. DOI: 10.1021/ja207798q.

(37) Martinolich, A. J.; Kurzman, J. A.; Neilson, J. R. Polymorph Selectivity of Superconducting CuSe2 Through Kinetic Control of Solid-State Metathesis. *J. Am. Chem. Soc.* **2015**, *137* (11), 3827-3833. DOI: 10.1021/ja512520z.

(38) Gilić, M.; Petrović, M.; Kostić, R.; Stojanović, D.; Barudžija, T.; Mitrić, M.; Romčević, N.; Ralević, U.; Trajić, J.; Romčević, M.; et al. Structural and optical properties of CuSe2 nanocrystals formed in thin solid Cu–Se film. *Infrared Physics & Technology* **2016**, *76*, 276-284. DOI: 10.1016/j.infrared.2016.03.008.

(39) Niu, G.; Lu, J.; Geng, J.; Li, S.; Zhang, H.; Xiong, W.; Ruan, Z.; Zhang, Y.; Fu, B.; Gao, L.; et al. Electronic properties of monolayer copper selenide with one-dimensional moiré patterns. *Front. Phys.* **2022**, *18* (1), 13303. DOI: 10.1007/s11467-022-1211-0.

(40) Kumar, M.; Rani, S.; Singh, Y.; Gour, K. S.; Singh, V. N. Tin-selenide as a futuristic material: properties and applications. *RSC Adv.* **2021**, *11* (12), 6477-6503. DOI: 10.1039/D0RA09807H.

(41) Izquierdo, E.; Robin, A.; Keuleyan, S.; Lequeux, N.; Lhuillier, E.; Ithurria, S. Strongly Confined HgTe 2D Nanoplatelets as Narrow Near-Infrared Emitters. *J. Am. Chem. Soc.* **2016**, *138* (33), 10496-10501. DOI: 10.1021/jacs.6b04429.

(42) Zhou, X.; Li, J.; Qian, X.; Zhu, J.; Kong, X.; Peng, X. Selective Formation of Monodisperse Right Trigonal-Bipyramidal and Cube-Shaped CdSe Nanocrystals: Stacking Faults and Facet-Ligand Pairing. *J. Am. Chem. Soc.* **2023**. DOI: 10.1021/jacs.3c07949.

(43) Murray, R. M.; Heyding, R. D. The Copper–Selenium System at Temperatures to 850 K and Pressures To 50 Kbar. *Can. J. Chem.* **1975**, *53* (6), 878-887. DOI: 10.1139/v75-122.

(44) Machado, K. D.; de Lima, J. C.; Grandi, T. A.; Campos, C. E. M.; Maurmann, C. E.; Gasperini, A. a. M.; Souza, S. M.; Pimenta, A. F. Structural study of Cu2−xSe alloys produced by mechanical alloying. *Acta Cryst B* **2004**, *60* (3), 282-286. DOI: 10.1107/S0108768104007475.

(45) Pai, R. R.; John, T. T.; Lakshmi, M.; Vijayakumar, K. P.; Sudha Kartha, C. Observation of phase transitions in chemical bath deposited copper selenide thin films through conductivity studies. *Thin Solid Films* **2005**, *473* (2), 208-212. DOI: 10.1016/j.tsf.2004.04.020.

(46) Thompson, K. L.; Katzbaer, R. R.; Terrones, M.; Schaak, R. E. Formation and Transformation of Cu2–xSe1–yTey Nanoparticles Synthesized by Tellurium Anion Exchange of Copper Selenide. *Inorganic Chemistry* **2023**, *62* (11), 4550-4557. DOI: 10.1021/acs.inorgchem.2c04467.

(47) Gariano, G.; Lesnyak, V.; Brescia, R.; Bertoni, G.; Dang, Z.; Gaspari, R.; De Trizio, L.; Manna, L. Role of the Crystal Structure in Cation Exchange Reactions Involving Colloidal Cu2Se Nanocrystals. *J. Am. Chem. Soc.* **2017**, *139* (28), 9583-9590. DOI: 10.1021/jacs.7b03706.

(48) Hernández-Pagán, E. A.; Robinson, E. H.; La Croix, A. D.; Macdonald, J. E. Direct Synthesis of Novel Cu2–xSe Wurtzite Phase. *Chem. Mater.* **2019**, *31* (12), 4619-4624. DOI: 10.1021/acs.chemmater.9b02019.

(49) Sims, C. E.; Barrera, G. D.; Allan, N. L.; Mackrodt, W. C. Thermodynamics and mechanism of the $B1$-$B2$ phase transition in group-I halides and group-II oxides. *Phys. Rev. B* **1998**, *57* (18), 11164-11172. DOI: 10.1103/PhysRevB.57.11164.

(50) Morgan, H. W. T.; Yamamoto, T.; Nishikubo, T.; Ohmi, T.; Koike, T.; Sakai, Y.; Azuma, M.; Ishii, H.; Kobayashi, G.; McGrady, J. E. Sequential Pressure-Induced B1–B2 Transitions in the Anion-Ordered Oxyhydride Ba2YHO3. *Inorganic Chemistry* **2022**, *61* (18), 7043-7050. DOI: 10.1021/acs.inorgchem.2c00465.

(51) Zhang, Y.; Shao, X.; Zheng, Y.; Yan, L.; Zhu, P.; Li, Y.; Xu, H. Pressure-induced structural transitions and electronic topological transition of Cu2Se. *Journal of Alloys and Compounds* **2018**, *732*, 280-285. DOI: 10.1016/j.jallcom.2017.10.201.

(52) Gao, X.; Zhang, X.; Zhao, L.; Huang, P.; Han, B.; Lv, J.; Qiu, X.; Wei, S.-H.; Tang, Z. Distinct Excitonic Circular Dichroism between Wurtzite and Zincblende CdSe Nanoplatelets. *Nano Letters* **2018**, *18* (11), 6665-6671. DOI: 10.1021/acs.nanolett.8b01001.

(53) Vinet, P.; Ferrante, J.; Rose, J. H.; Smith, J. R. Compressibility of solids. *Journal of Geophysical Research: Solid Earth* **1987**, *92* (B9), 9319-9325. DOI: 10.1029/JB092iB09p09319.

(54) Jeanloz, R. Universal equation of state. *Phys. Rev. B* **1988**, *38* (1), 805-807. DOI: 10.1103/PhysRevB.38.805.

(55) Takemura, K.; Dewaele, A. Isothermal equation of state for gold with a He-pressure medium. *Phys. Rev. B* **2008**, *78* (10), 104119. DOI: 10.1103/PhysRevB.78.104119.

(56) Bertolotti, F.; Dirin, D. N.; Ibáñez, M.; Krumeich, F.; Cervellino, A.; Frison, R.; Voznyy, O.; Sargent, E. H.; Kovalenko, M. V.; Guagliardi, A.; et al. Crystal symmetry breaking and vacancies in colloidal lead chalcogenide quantum dots. *Nature Materials* **2016**, *15* (9), 987-994. DOI: 10.1038/nmat4661.

(57) Beimborn, J. C., II; Walther, L. R.; Wilson, K. D.; Weber, J. M. Size-Dependent Pressure-Response of the Photoluminescence of CsPbBr3 Nanocrystals. *The Journal of Physical Chemistry Letters* **2020**, *11* (5), 1975-1980. DOI: 10.1021/acs.jpclett.0c00174.

(58) Toby, B. H.; Von Dreele, R. B. GSAS-II: the genesis of a modern open-source all purpose crystallography software package. *J Appl Cryst* **2013**, *46* (2), 544-549. DOI: 10.1107/S0021889813003531.